

広島大学学術情報リポジトリ  
Hiroshima University Institutional Repository

Title	Porosity Engineering of Pt-Loaded Nb-SnO <sub>2</sub> Catalyst Layers in Polymer Electrolyte Fuel Cells
Author(s)	Hirano, Tomoyuki; Tsuboi, Takama; Ho, Thi Thanh Nguyen; Tanabe, Eishi; Takano, Aoi; Kataoka, Mikihiro; Ogi, Takashi
Citation	ACS Applied Energy Materials , 6 (24) : 12364 - 12370
Issue Date	2023-12-08
DOI	
Self DOI	
URL	<a href="https://ir.lib.hiroshima-u.ac.jp/00055910">https://ir.lib.hiroshima-u.ac.jp/00055910</a>
Right	<p>This document is the Accepted Manuscript version of a Published Work that appeared in final form in ACS Applied Energy Materials, copyright © American Chemical Society after peer review and technical editing by the publisher. To access the final edited and published work see <a href="https://doi.org/10.1021/acsaem.3c02165">https://doi.org/10.1021/acsaem.3c02165</a></p> <p>This is not the published version. Please cite only the published version.</p> <p>この論文は出版社版ではありません。引用の際には出版社版をご確認、ご利用ください。</p>
Relation	



# Porosity Engineering of Pt Loaded Nb-SnO<sub>2</sub> Catalyst Layers in Polymer Electrolyte Fuel Cells

*Tomoyuki Hirano,<sup>\*,1</sup> Takama Tsuboi,<sup>1</sup> Thi Thanh Nguyen Ho,<sup>1</sup> Eishi Tanabe,<sup>2</sup> Aoi Takano,<sup>3</sup>  
Mikihiro Kataoka,<sup>3</sup> and Takashi Ogi<sup>\*,1</sup>*

<sup>1</sup> Chemical Engineering Program, Graduate School of Advanced Science and Engineering,  
Hiroshima University, 1-4-1 Kagamiyama, Higashi-Hiroshima, Hiroshima 739-8527, Japan

<sup>2</sup> Hiroshima Prefectural Institute of Industrial Science and Technology, 3-10-31 Kagamiyama,  
Higashi Hiroshima, Hiroshima 739-0046, Japan.

<sup>3</sup> Cataler Corporation, 7800 Chihama, Kakegawa, Shizuoka 437-1492, Japan

## ABSTRACT

Recently, the emphasis in hydrogen-fuel utilization technologies—particularly polymer-electrolyte fuel cells (PEFCs)—has recently shifted from light-duty to heavy-duty vehicles. There is consequently an urgent need to develop a catalyst with excellent durability. In this study, we have endeavored to improve the power-generating performance of PEFCs by using high durability Nb-SnO<sub>2</sub> (NTO) nanoparticles and by controlling the porosity of the catalyst layer. We tuned the fused-aggregate network structure of the NTO nanoparticles by annealing them at 1000°C or 1200°C. This treatment promoted the development of aggregated structures of the NTO nanoparticles, which resulted in an increase in the porosity of the catalyst layer. In these catalysts, the maximum current density increased with increasing porosity. The gas-diffusion resistance calculated from the current-voltage (*I-V*) characteristics declined from 148 m/s for NTO nanoparticles before annealing, to 113 m/s after annealing at 1000°C, and to 102 m/s after annealing at 1200°C. This study thus demonstrates that high-performance catalysts with high durability for PEFCs can be achieved by precisely engineering the porosity of the catalyst layer.

## KEYWORDS

Polymer electrolyte fuel cell, Nb-doped SnO<sub>2</sub>, Porosity, Oxide support, Flame synthesis

## Introduction

Polymer-electrolyte fuel cells (PEFCs) are being explored extensively for use in various types of mobile applications as next-generation power-generating systems with low environmental

impact<sup>1-6</sup>. Platinum-loaded carbon (Pt/C) is generally chosen as the catalyst in a PEFC because carbon is a catalyst support with a high electrical conductivity and a high specific surface area<sup>7</sup>. In addition, the porosity of its unique network structure plays a crucial role in a PEFC system by enabling both the diffusion of gas and the removal of water produced in the cell<sup>8, 9</sup>. However, the degradation of carbon under the high operating potentials in PEFCs has become a serious issue, and it is necessary to improve the durability of the catalyst support to expand the range of applications to heavy-duty vehicles<sup>3, 10</sup>. For this reason, thermally and chemically stable conductive ceramic supports are currently under development<sup>11-15</sup>.

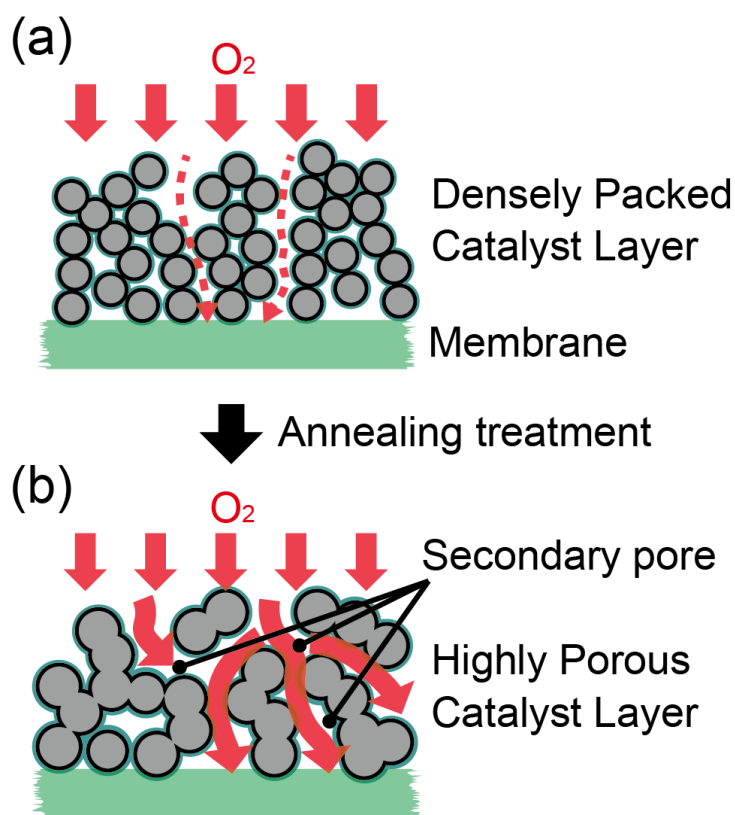
Nb-doped tin oxide (Nb–SnO<sub>2</sub>: NTO) has also been developed as a catalyst support for PEFCs, and it exhibits both high electrochemical activity and high durability<sup>16-20</sup>. In most cases, a flame process is used to produce Nb–SnO<sub>2</sub> nanoparticles. In such a process, the raw precursor material is introduced into a flame in a gas phase to obtain fine particles<sup>21-24</sup>. The structures of flame-made fine particles can be controlled precisely by adjusting the type of solvent and by changing the combustion method<sup>25-32</sup>. Using this method, Nb–SnO<sub>2</sub> nanoparticles have been synthesized in a network structure in which the particles are fused together, and this material has been used as an electrocatalyst. For example, Kakinuma et al. have reported the synthesis of NTO nanoparticles and their application as catalyst supports for PEFC cathodes with improved durability<sup>33</sup>. The flame method has also been employed to fabricate NTO nanoparticles in a fused-aggregate network structure, enhancing both the electrical conductivity and the gas diffusivity of the material. Hirano et al. prepared Pt-loaded NTO nanoparticles in a one-step process using a flame method and evaluated their electrochemical properties<sup>19</sup>. The use of spray combustion, in which the precursor solution is burned directly, promotes gasification of the precursor and enables the uniform deposition of Pt nanoparticles on the NTO particles. In

addition, NTO nanoparticles with high specific surface areas have been prepared by adjusting the combustion conditions, and the fuel-cell properties were determined using a single cell<sup>20</sup>.

The main component of a PEFC is a membrane–electrode assembly (MEA) consisting of a polymer–electrolyte membrane and a porous electrode coated with catalysts, which performs hydrogen oxidation at the anode and oxygen reduction at the cathode. Conventionally, catalyst electrodes are hot-pressed onto both sides of a proton-exchange membrane at high pressure and relatively high temperature (i.e., using the hot-press technique)<sup>34</sup>. In our previous studies, we found that MEAs with Pt/NTO catalysts fabricated using the hot-press method have densely packed catalyst layers and lower porosity than conventional carbon supports<sup>20</sup>. Current–voltage ( $I$ – $V$ ) measurements show that—compared to a carbon support—an NTO support exhibits both a voltage drop in the high-current region and increased gas-diffusion resistance. The presence of pores within the catalyst layer is critical to its effectiveness, acting as channels through which reactant gases access the catalytic interface. These pores play a crucial role in water management, orchestrating the removal of excess water produced during the oxygen reduction reaction while ensuring that the membranes and ionomers remain adequately hydrated. Therefore, engineering the porosity of the catalyst layer in an MEA is essential for improving the performance of PEFCs using NTO supports.

In this study, we synthesized NTO nanoparticles using flame-spray pyrolysis (FSP), and we increased the porosity of the catalyst layer by changing the network structure of the nanoparticles using an annealing treatment. A conceptual illustration of the porosity engineering of the catalyst layer using an annealing treatment is shown in Scheme 1. When a catalyst layer is prepared using NTO nanoparticles, the particles are densely packed, and they have a poorly developed particle necking structure (Scheme 1a). Such a densely packed particle-layer structure hinders efficient

fluid transport (e.g., the diffusion of oxygen), which is necessary for power generation, leading to a reduction in voltage. However, if the NTO nanoparticles can be annealed to bridge the particles together before making the catalyst layer, secondary pores may form between the particles (Scheme 1b). We expect the secondary pores so produced to increase the mean pore size of the catalyst layer, promoting mass transport of fluids and improving power-generating performance. We therefore fabricated MEAs using structure-controlled NTO nanoparticles, and we quantified the porosity of the MEAs by binarizing electron microscope images. We evaluated the fuel cell performance using a single cell, and we also evaluated the effect of the nanostructure of the NTO nanoparticles on the  $I-V$  characteristics.



**Scheme 1.** Conceptual illustration of porosity engineering using an annealing treatment; see text.

## **Experimental**

### **Catalyst synthesis**

We prepared NTO nanoparticles using FSP<sup>20</sup>. We procured C<sub>16</sub>H<sub>30</sub>O<sub>4</sub>Sn and Nb(OC<sub>2</sub>H<sub>5</sub>)<sub>5</sub> from Sigma–Aldrich Co. in the USA. To prepare the precursor solution, we dissolved these chemicals in xylene obtained from Sigma–Aldrich Co. The concentrations of Sn and Nb in the solution were both 0.1 mol/L, with Nb accounting for 4% of the total number of atoms. We dispensed the solution through a syringe pump and atomized it using a two-fluid nozzle—model AM6 (ATOMAX Co., Shizuoka, Japan)—at a flow rate of 3 mL/min in the presence of oxygen (1.5 L/min). We then burned the atomized solution in a premixed methane/air flame (1.2 L/min of methane and 10 L/min of air) to form a spray flame. We collected the particles so produced on a polytetrafluoroethylene (PTFE) membrane filter. We then annealed the as-prepared NTO particles inside a tubular furnace. We heated the flame-made particles to various temperatures at a heating rate of 400°C/h in air. After the annealing treatment, the particles were allowed to cool naturally. We loaded the Pt catalysts onto the NTO nanoparticles using the liquid-phase reduction method described in earlier papers<sup>20</sup>. The nominal loading amount of Pt nanoparticles was 20 wt%.

### **Materials characterization**

We observed the morphologies of the prepared particles using a field emission scanning electron microscope (FE–SEM; S-5200, Hitachi High-Tech. Corp., Tokyo, Japan). We also performed transmission electron microscopy (TEM) using a JEOL 297 kV JEM-3000F. We obtained cross-

sectional SEM images by using a focused-ion-beam (FIB) system with a  $\text{Xe}^+$  plasma to produce a cleanly cut cross-section, employing an FEI Helios PFIB Dual Beam FIB–SEM. We also investigated the crystal structures of the particles using powder X-ray diffraction (XRD), employing a Bruker D2 PHASER model apparatus (Billerica, Massachusetts, USA) operated at 40 kV and 30 mA. We determined the specific surface areas from nitrogen adsorption–desorption isotherms obtained at 77 K using a BELSORP-max instrument model. We performed pore-size characterizations using mercury porosimetry.

### **Electrochemical measurements**

We produced the catalyst inks for the cathodes by using a homogenizer to mix together the Pt/NTO catalyst, Nafion ionomers from Wako Pure Chemical Industries Ltd. (Osaka, Japan), ethanol, and purified water to obtain an ionomer/support (I/S) volume ratio of 0.175. We loaded 0.1  $\text{mg}/\text{cm}^2$  of Pt onto each cathode. We used Pt/C (Pt loading 20 wt%; Ketjenblack ECP from Lion Specialty Chemicals Co., Ltd., Tokyo, Japan) for the anodes in all the test cells. We used a commercial carbon-supported Pt catalyst (XC-72R, Cabot Corporation, Waltham, MA, USA) for reference for the cathode measurements. We prepared the catalyst inks for the anodes similarly. For the anode electrodes, the Pt loading was around 0.1  $\text{mg}/\text{cm}^2$ , and the I/S ratio was about 1.0. We prepared the membrane–electrode assembly (MEA) using a decal-transfer technique. This involved hot-pressing anode and cathode catalyst layers that had been coated onto PTFE sheets onto a Nafion membrane at a temperature of 126°C and a pressure of 10 MPa. The geometric area of the electrodes was 1.0  $\text{cm}^2$ . We placed the MEA into a homemade single-cell holder with straight-line gas-flow channels. We measured the cell potential as a function of current density at

a cell temperature of 60°C and a relative humidity of 100%. We introduced hydrogen gas to the anode and air to the cathode. The back-pressures for both the cathode and anode were 108 kPa. The gas-flow rate at the cathode was 1.0 L/min while that at the anode was 0.5 L/min. We carried out a pre-conditioning process before performing the main measurements, executing 40 pre-conditioning cycles at 0.1 V/s over the range 0–1.0 V. We also carried out AC-impedance measurements from 100 kHz to 0.1 Hz at a potential of 0.4 V and an amplitude of 0.02 V. The cells and MEAs used for these measurements were the same as for the output measurements. The temperature, humidity, and back pressure also were the same as for the output measurements, but those measurements were performed under non-power-generating conditions. We measured the current–voltage curves potentiostatically at 0.01 V/s in the range 0–1.0 V. To evaluate the electrochemical characteristics, we performed cyclic voltammetry (CV) with a reversible hydrogen electrode as the reference electrode. The electrochemical measurement steps and CV conditions are described elsewhere<sup>20</sup>.

## **Results and discussion**

We first evaluated the effects of the annealing conditions on the crystal structure of the NTO nanoparticles. Figure 1 shows the XRD patterns of the NTO nanoparticles synthesized under each annealing condition. The NTO nanoparticles synthesized using FSP without annealing showed a similar pattern, which we attribute to the tetragonal structure of tin oxide; detailed crystallographic parameters have been determined by Hirano et al. for similar flame-made NTO nanoparticles<sup>20</sup>. Additionally, it has been demonstrated that niobium is distributed homogeneously within the NTO nanoparticles and that it is in a pentavalent valence state.

Annealing of the flame-made particles did not result in significant changes in the crystal structure, regardless of the temperature or duration of the annealing treatment. However, the sharpness of the XRD peaks increased with increasing annealing temperature, indicating that the crystallinity had been improved. We evaluated the crystallinity quantitatively by calculating the crystallite size  $D_c$  using the Scherrer equation. The crystallite size increased from 9.95 nm to 19.80 nm as we increased the annealing temperature, confirming that the crystallinity had improved. At an annealing temperature of 1200°C, the crystallite size remained unchanged at around 21 nm, even with annealing times as long as 2 h or 4 h. For Nb–SnO<sub>2</sub>, it is thus clear that the annealing temperature has a more significant effect on the crystallinity than does the annealing time.

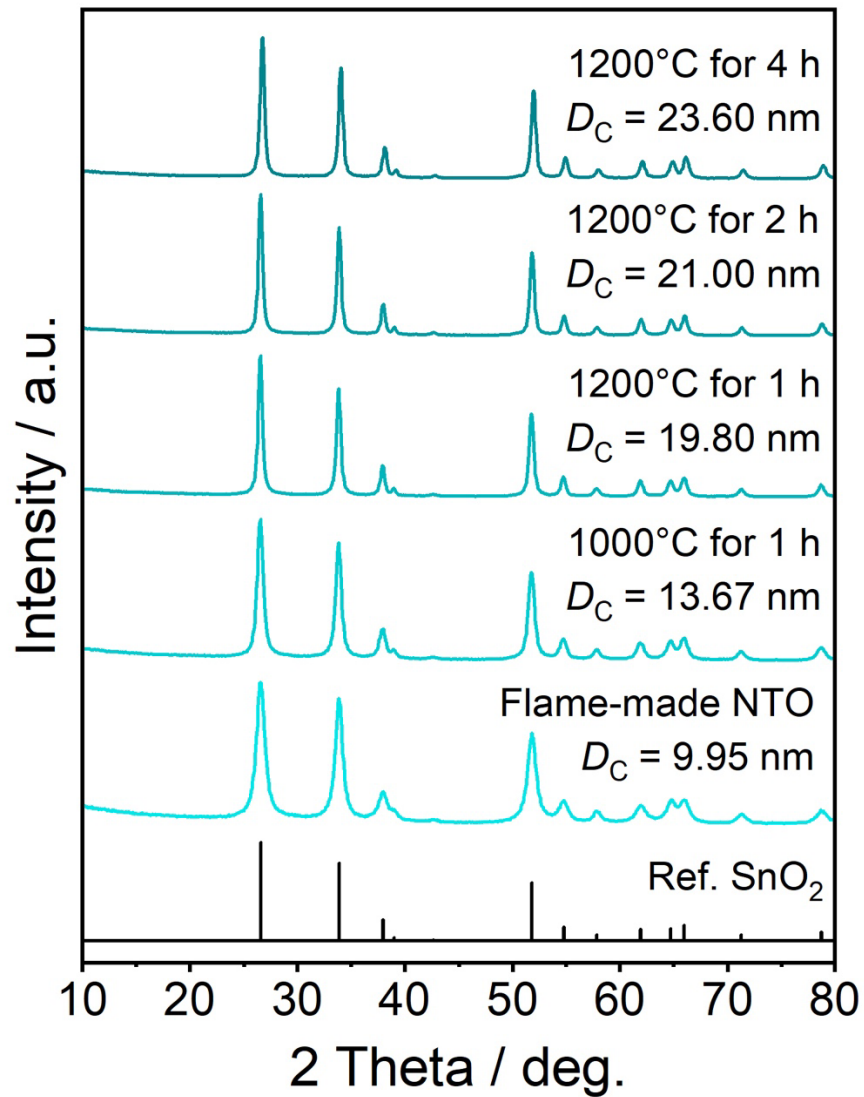


**Figure 1.** The XRD patterns of flame-made NTO nanoparticles before and after annealing at 1000°C for 1 h and at 1200°C for 1 h, 2 h, and 4 h.

Next, we evaluated the effects of the annealing conditions on the morphologies of the NTO nanoparticles, and Figure 2 shows SEM images of the NTO nanoparticles synthesized under each annealing condition. For reference, we also observed the morphology of carbon black, which is

commonly used as a catalyst support in PEFCs. Carbon black has a unique network structure, with interconnected particles, each several tens of nm in size. Such structures produce secondary macropores that act as flow paths for gases and liquids when used in PEFCs. The interconnected particles also reduce the resistance at particle boundaries, improving the electrical conductivity<sup>17</sup>. Flame-generated NTO nanoparticles that have not been annealed have a network structure that is similar to that of carbon. This structure is formed by the bonding of the nanoparticles in the high-temperature region of the flame. The mean particle size increased after annealing at either 1000°C or 1200°C. After annealing, the particle morphology of the network structure was maintained, and only the mean particle diameter changed. We calculated the particle size from TEM images using the Ferret diameter, and we prepared a particle-size distribution by counting more than 500 particles (Figure S1 in Supporting Information). The geometric mean diameter increased from 9.54 nm to 28.16 nm as we increased the annealing temperature and time.

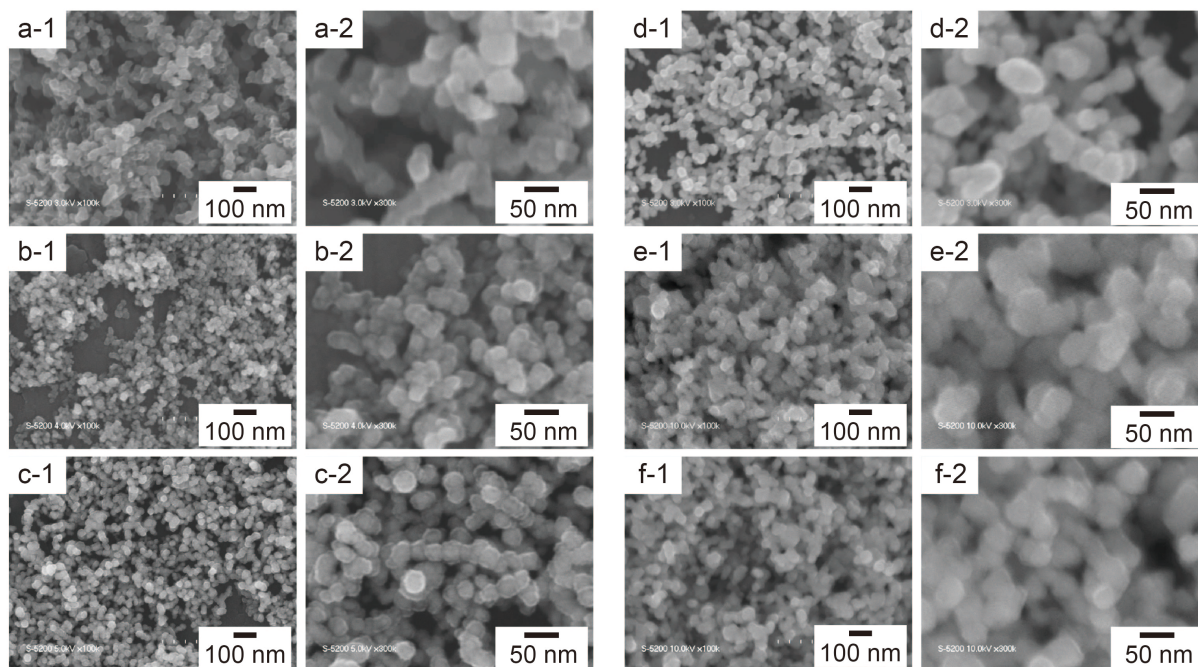


**Figure 2.** SEM images of (a) carbon nanoparticles and of flame-made NTO nanoparticles (b) before annealing and after annealing at (c) 1000°C for 1 h, (d) at 1200°C for 1 h, (e) at 1200°C for 2 h, and (f) at 1200°C for 4 h.

We next measured the specific surface area using the Brunauer–Emmett–Teller (BET) method. We used the density of tin oxide ( $6.95 \text{ g/cm}^3$ ) to calculate the BET equivalent particle diameter. Table 1 summarizes the BET specific surface area ( $S_{\text{BET}}$ ), BET equivalent particle diameter ( $d_{\text{BET}}$ ), crystal size ( $d_{\text{XRD}}$ ), and particle size measured from TEM ( $d_{\text{TEM}}$ ) for NTO nanoparticles annealed under each condition. The crystallite size and particle size measured using TEM are almost identical, indicating that the particles are almost perfect single crystals. We observed a similar trend for all particle-size calculation methods, with the particle size increasing with increasing annealing temperature and with no effect of the annealing time. Notably, the BET equivalent particle diameter is calculated to be more significant than the XRD or TEM particle

diameters. In the actual samples, the particles have an aggregated necking structure, which reduces the specific surface area. As a result, particle diameters calculated from the specific surface area tend to be larger than those calculated using XRD or TEM. In other words, the tendency for the BET equivalent particle diameter to be larger than the XRD and TEM diameters implies the development of particle necking compared with the isolated particle state.

**Table 1.** Comparison of the sizes of prepared particles obtained using BET, XRD, and TEM.

Samples	$S_{\text{BET}}$ ( $\text{m}^2/\text{g}$ )	$d_{\text{BET}}$ (nm)	$d_{\text{XRD}}$ (nm)	$d_{\text{TEM}}$ (nm)
Flame-made NTO	65.72	13.14	9.95	9.54
NTO (1000°C, 1 h)	45.68	18.90	13.67	15.81
NTO (1200°C, 1 h)	30.41	28.39	19.80	20.56
NTO (1200°C, 2 h)	27.77	31.09	21.00	24.94
NTO (1200°C, 4 h)	23.30	37.05	23.60	28.16

Figure 3 shows the pore-size distributions of the NTO nanoparticles obtained using mercury porosimetry. For the annealed samples, the peaks shift to the right, indicating increased pore sizes. The average pore size (mode diameter) was 10.6 nm before annealing, whereas it was 24.88 nm after annealing at 1000°C and 47.49 nm after annealing at 1200°C. The average pore size tended to approach that of carbon (66.0 nm) as the annealing temperature was increased. As described above, the annealing treatment increased the particle size while maintaining the necking structure. As a result, the sizes of secondary pores generated by the necking structures of the particles increased.

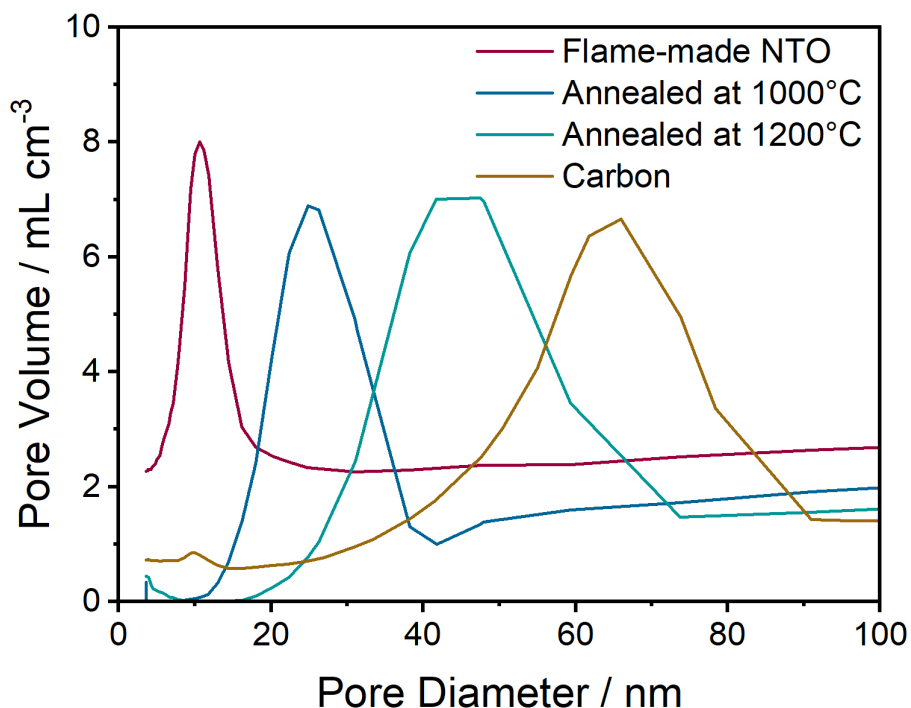


**Figure 3.** Pore-size distribution of carbon nanoparticles and of flame-made NTO nanoparticles before and after annealing at 1000°C and 1200°C.

Figure 4 shows cross-sectional SEM images of MEAs fabricated using NTO nanoparticles synthesized under each condition. To simplify the cross-section observations, the Pt catalyst is not supported here. We observed a catalyst layer about 7–8  $\mu\text{m}$  thick in each case. The carbon-nanoparticle MEAs exhibit numerous macropores formed by the strong network structure of the particles. However, the flame-made NTO nanoparticles that have not been annealed have a less-developed structure, so these catalyst layers are compressed by hot-pressing. These images confirm that the pores in the catalyst layer are increased by annealing the layer at 1000°C or 1200°C. As mentioned above, the annealing treatment increases the particle size, which increases the framework strength of the necking structure. The increased pore size measured using

mercury porosimetry may also be due to this effect. To evaluate the porosity of the catalyst layer in the MEA quantitatively, we sliced the catalyst layer using an FIB to obtain a cross-section, and we calculated the porosity by binarizing the SEM image using ImageJ<sup>35</sup>. The porosity of the carbon layer was 37.98%, which provides a quantitative measure of the secondary pores generated by the characteristic necking structure of carbon. The non-annealed NTOs shown in Figure 4 (b-2) are very densely packed, with few pores inside the catalyst layer and small pore sizes. The resolution of the FIB–SEM image was insufficient to analyze them in detail, so we were not able to calculate a reliable porosity for the non-annealed NTO nanoparticles. However, we confirmed that they achieved a porosity of 36.52% when they were annealed at 1000°C and of 44.01% when annealed at 1200°C. These porosities are comparable to or larger than that of carbon.

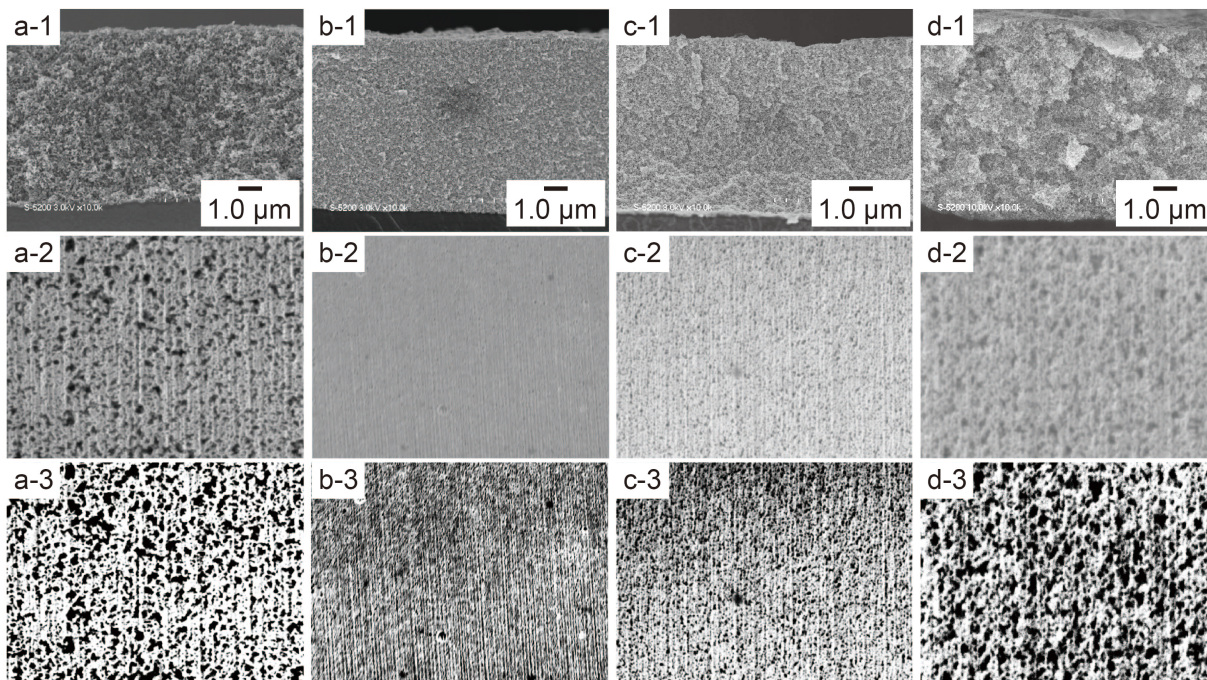


**Figure 4.** Cross-sectional SEM images of catalyst layers (a) using carbon nanoparticles and using flame-made NTO nanoparticles (b) before annealing and after annealing at (c) 1000°C and (d) 1200°C. (1, SEM image; 2, FIB–SEM image; 3, FIB–SEM image after binarization).

We loaded the Pt catalysts onto the synthesized NTO nanoparticles using the liquid-phase method, and we evaluated the  $I$ – $V$  characteristics of a single cell. The  $I$ – $V$  characteristics of each catalyst are shown in Figure 5. The Pt/C catalysts we measured for reference showed the best performance. We attribute this to the existence of numerous mesopores in the carbon and to a large number of secondary pores in the network structure, which allow effective utilization of the Pt catalysts. For the Pt/NTO nanoparticles, the maximum current density increased as we increased the annealing temperature. The annealing process increases the porosity of the catalyst layer—as demonstrated both by mercury porosimetry and by the cross-sectional MEA

observations—which allows efficient gas transport and the removal of the water generated. We calculated various resistances from the  $I$ - $V$  characteristics. The gas-diffusion resistance was 148 m/s for the NTO nanoparticles before annealing, 113 m/s after annealing at 1000°C, and 102 m/s after annealing at 1200°C. However, the current-cutoff resistance was 66 mΩ for the NTO nanoparticles before annealing, and it increased to 89 mΩ after annealing at 1000°C and to 103 mΩ after annealing at 1200°C. The increase in the NTO nanoparticle size may have decreased the dispersion of the Pt catalyst, resulting in lower power-generating performance in the low-current region.

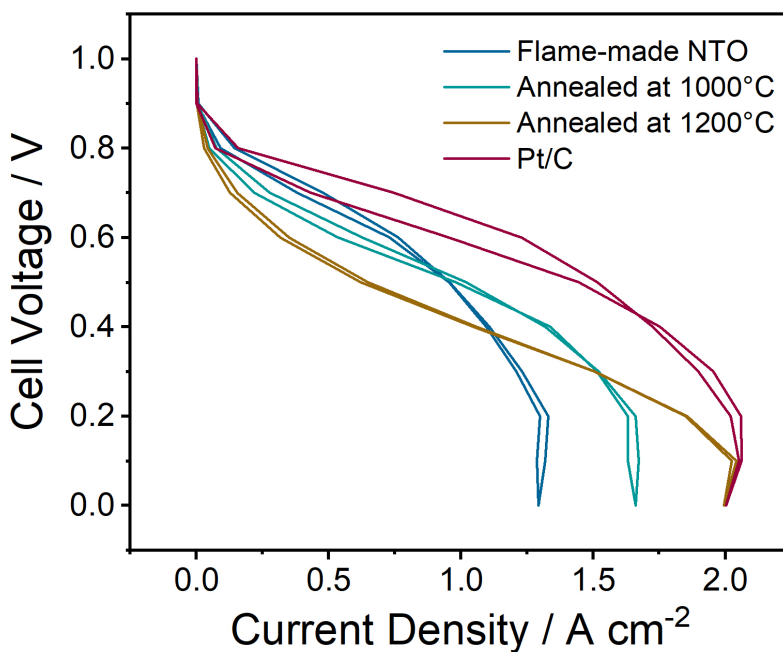


**Figure 5.** The  $I$ - $V$  characteristics of membrane-electrode assemblies using Pt/C and using Pt deposited on flame-made NTO nanoparticles before and after annealing at 1000°C and at 1200°C.

## **Conclusion**

In this study, we attempted to increase the porosity of the catalyst layer in an MEA by using nanostructure-controlled Pt/NTO nanoparticles to improve the PEFC performance. We annealed the NTO nanoparticles that had been synthesized using the flame method to control their nanostructures. The flame-made NTO nanoparticles had a mean particle size of 9.54 nm, and the particles were connected to each other in a network structure. Cross-sectional images of the catalyst layers showed quantitatively that the porosity of the catalyst layer increased as we increased the annealing temperature. We evaluated the power-generating performance using a single cell, and we confirmed that the maximum current density increased as the porosity of the catalyst layer increased. However, the mean particle size also increased with increasing porosity, which resulted in a voltage drop in the low-current region. Based on the results of this study, we conclude that the power-generating performance of MEAs containing NTO nanoparticles can be improved by increasing the porosity of the catalyst layer of the MEA. In the future, it will be necessary to develop techniques to suppress the increase in the mean particle size while increasing the porosity.

## **Supporting Information**

TEM images of flame-made NTO nanoparticles before annealing and after annealing.

## **AUTHOR INFORMATION**

### **Corresponding Author**

\* Tomoyuki Hirano; Email: tomoyuki-hirano@hiroshima-u.ac.jp; Phone: +81-82-424-7850

\* Takashi Ogi; Email: ogit@hiroshima-u.ac.jp; Phone: +81-82-424-3765

## ACKNOWLEDGMENT

This work was supported by JSPS KAKENHI Grant Numbers JP22K20482, JP23K13590 (T.H), and JP23H01745 (T.O.). This work was partly supported by the Center for Functional Nano Oxides at Hiroshima University, the International Network on Polyoxometalate Science, the JSPS Core-to-Core Program, the Information Center of Particle Technology, Japan, and the Hosokawa Powder Technology Foundation. The authors thank the Natural Science Center for Basic Research and Development (N-BARD) for access to SEM facilities.

## References

- (1) Suter, T. A. M.; Smith, K.; Hack, J.; Rasha, L.; Rana, Z.; Angel, G. M. A.; Shearing, P. R.; Miller, T. S.; Brett, D. J. L. Engineering Catalyst Layers for Next - Generation Polymer Electrolyte Fuel Cells: A Review of Design, Materials, and Methods. *Advanced Energy Materials* **2021**, *11* (37), 2101025. DOI: 10.1002/aenm.202101025.
- (2) Zhang, J.; Yuan, Y.; Gao, L.; Zeng, G.; Li, M.; Huang, H. Stabilizing Pt-Based Electrocatalysts for Oxygen Reduction Reaction: Fundamental Understanding and Design Strategies. *Adv. Mater.* **2021**, *33* (20), e2006494. DOI: 10.1002/adma.202006494.
- (3) Cullen, D. A.; Neyerlin, K. C.; Ahluwalia, R. K.; Mukundan, R.; More, K. L.; Borup, R. L.; Weber, A. Z.; Myers, D. J.; Kusoglu, A. New roads and challenges for fuel cells in heavy-duty transportation. *Nature Energy* **2021**, *6* (5), 462-474. DOI: 10.1038/s41560-021-00775-z.

- (4) Balgis, R.; Widiyastuti, W.; Ogi, T.; Okuyama, K. Enhanced Electrocatalytic Activity of Pt/3D Hierarchical Bimodal Macroporous Carbon Nanospheres. *ACS Appl Mater Interfaces* **2017**, *9* (28), 23792-23799. DOI: 10.1021/acsami.7b05873.
- (5) Balgis, R.; Arif, A. F.; Mori, T.; Ogi, T.; Okuyama, K.; Anilkumar, G. M. Morphology-dependent electrocatalytic activity of nanostructured Pt/C particles from hybrid aerosol-colloid process. *AIChE J.* **2016**, *62* (2), 440-450. DOI: 10.1002/aic.15059.
- (6) Balgis, R.; Anilkumar, G. M.; Sago, S.; Ogi, T.; Okuyama, K. Nanostructured design of electrocatalyst support materials for high-performance PEM fuel cell application. *J. Power Sources* **2012**, *203*, 26-33. DOI: 10.1016/j.jpowsour.2011.11.064.
- (7) Lee, M.; Uchida, M.; Tryk, D. A.; Uchida, H.; Watanabe, M. The effectiveness of platinum/carbon electrocatalysts: Dependence on catalyst layer thickness and Pt alloy catalytic effects. *Electrochim. Acta* **2011**, *56* (13), 4783-4790. DOI: 10.1016/j.electacta.2011.03.072.
- (8) Kartouzian, D.; Mohseninia, A.; Markötter, H.; Langner, P.; Scholta, J.; Manke, I. Impact of porosity gradients within catalyst layer and MPL of a PEM fuel cell on the water management and performance: a neutron radiography investigation. *ECS Transactions* **2019**, *92* (8), 135.
- (9) Soboleva, T.; Malek, K.; Xie, Z.; Navessin, T.; Holdcroft, S. PEMFC catalyst layers: the role of micropores and mesopores on water sorption and fuel cell activity. *ACS Appl Mater Interfaces* **2011**, *3* (6), 1827-1837. DOI: 10.1021/am200590w From NLM Medline.
- (10) Forouzandeh, F.; Li, X.; Banham, D. W.; Feng, F.; Ye, S.; Birss, V. Understanding the Corrosion Resistance of Meso- and Micro-Porous Carbons for Application in PEM Fuel Cells. *J. Electrochem. Soc.* **2018**, *165* (6), F3230-F3240. DOI: 10.1149/2.0261806jes.

- (11) Ioroi, T.; Siroma, Z.; Fujiwara, N.; Yamazaki, S.-i.; Yasuda, K. Sub-stoichiometric titanium oxide-supported platinum electrocatalyst for polymer electrolyte fuel cells. *Electrochem. Commun.* **2005**, *7* (2), 183-188. DOI: 10.1016/j.elecom.2004.12.007.
- (12) Sasaki, K.; Takasaki, F.; Noda, Z.; Hayashi, S.; Shiratori, Y.; Ito, K. Alternative Electrocatalyst Support Materials for Polymer Electrolyte Fuel Cells. *ECS Transactions* **2010**, *33* (1), 473-482. DOI: 10.1149/1.3484545.
- (13) Abdullah, N.; Kamarudin, S. K. Titanium dioxide in fuel cell technology: An overview. *J. Power Sources* **2015**, *278*, 109-118. DOI: 10.1016/j.jpowsour.2014.12.014.
- (14) Geiger, S.; Kasian, O.; Mingers, A. M.; Mayrhofer, K. J. J.; Cherevko, S. Stability limits of tin-based electrocatalyst supports. *Sci Rep* **2017**, *7* (1), 4595. DOI: 10.1038/s41598-017-04079-9  
From NLM PubMed-not-MEDLINE.
- (15) Zhang, Z.; Liu, J.; Gu, J.; Su, L.; Cheng, L. An overview of metal oxide materials as electrocatalysts and supports for polymer electrolyte fuel cells. *Energy Environ. Sci.* **2014**, *7* (8), 2535-2558. DOI: 10.1039/c3ee43886d.
- (16) Takasaki, F.; Matsuie, S.; Takabatake, Y.; Noda, Z.; Hayashi, A.; Shiratori, Y.; Ito, K.; Sasaki, K. Carbon-Free Pt Electrocatalysts Supported on SnO<sub>2</sub> for Polymer Electrolyte Fuel Cells: Electrocatalytic Activity and Durability. *J. Electrochem. Soc.* **2011**, *158* (10), B1270-B1275. DOI: 10.1149/1.3625918.
- (17) Kakinuma, K.; Suda, K.; Kobayashi, R.; Tano, T.; Arata, C.; Amemiya, I.; Watanabe, S.; Matsumoto, M.; Imai, H.; Iiyama, A.; Uchida, M. Electronic States and Transport Phenomena of Pt Nanoparticle Catalysts Supported on Nb-Doped SnO<sub>2</sub> for Polymer Electrolyte Fuel Cells. *ACS Appl Mater Interfaces* **2019**, *11* (38), 34957-34963. DOI: 10.1021/acsami.9b11119.

- (18) Shi, G.; Tano, T.; Tryk, D. A.; Iiyama, A.; Uchida, M.; Kakinuma, K. Temperature Dependence of Oxygen Reduction Activity at Pt/Nb-Doped SnO<sub>2</sub> Catalysts with Varied Pt Loading. *ACS Catalysis* **2021**, *11* (9), 5222-5230. DOI: 10.1021/acscatal.0c05157.
- (19) Hirano, T.; Tsuboi, T.; Tanabe, E.; Ogi, T. In-situ flame deposition of Pt catalysts on Nb-doped SnO<sub>2</sub> nanoparticles. *J. Alloys Compd.* **2022**, *898*, 162749. DOI: 10.1016/j.jallcom.2021.162749.
- (20) Hirano, T.; Tsuboi, T.; Cao, K. L. A.; Tanabe, E.; Ogi, T. High specific surface area niobium-doped tin oxide nanoparticles produced in spray flames as catalyst supports in polymer electrolyte fuel cells. *J. Nanopart. Res.* **2023**, *25*, 1.
- (21) Pokhrel, S.; Madler, L. Flame-made Particles for Sensors, Catalysis, and Energy Storage Applications. *Energy Fuels* **2020**, *34* (11), 13209-13224. DOI: 10.1021/acs.energyfuels.0c02220.
- (22) Li, S.; Ren, Y.; Biswas, P.; Tse, S. D. Flame aerosol synthesis of nanostructured materials and functional devices: Processing, modeling, and diagnostics. *Prog. Energy Combust. Sci.* **2016**, *55*, 1-59. DOI: 10.1016/j.peccs.2016.04.002.
- (23) Teoh, W. Y.; Amal, R.; Madler, L. Flame spray pyrolysis: An enabling technology for nanoparticles design and fabrication. *Nanoscale* **2010**, *2* (8), 1324-1347. DOI: 10.1039/c0nr00017e.
- (24) Mädler, L.; Kammler, H. K.; Mueller, R.; Pratsinis, S. E. Controlled synthesis of nanostructured particles by flame spray pyrolysis. *J. Aerosol Sci* **2002**, *33* (2), 369-389.
- (25) Hirano, T.; Nakakura, S.; Rinaldi, F. G.; Tanabe, E.; Wang, W.-N.; Ogi, T. Synthesis of highly crystalline hexagonal cesium tungsten bronze nanoparticles by flame-assisted spray pyrolysis. *Adv. Powder Technol.* **2018**, *29* (10), 2512-2520. DOI: 10.1016/j.appt.2018.07.001.

- (26) Hirano, T.; Kikkawa, J.; Rinaldi, F. G.; Kitawaki, K.; Shimokuri, D.; Tanabe, E.; Ogi, T. Tubular Flame Combustion for Nanoparticle Production. *Industrial & Engineering Chemistry Research* **2019**, *58* (17), 7193-7199. DOI: 10.1021/acs.iecr.9b00620.
- (27) Dani Nandiyanto, A. B.; Kito, Y.; Hirano, T.; Ragadhita, R.; Le, P. H.; Ogi, T. Spherical submicron YAG:Ce particles with controllable particle outer diameters and crystallite sizes and their photoluminescence properties. *RSC Advances* **2021**, *11* (48), 30305-30314. DOI: 10.1039/d1ra04800g.
- (28) Hirano, T.; Kikkawa, J.; Shimokuri, D.; Nandiyanto, A. B. D.; Ogi, T. Sinter-Necked, Mixed Nanoparticles of Metallic Tungsten and Tungsten Oxide Produced in Fuel-Rich Methane/Air Tubular Flames. *J. Chem. Eng. Jpn.* **2021**, *54* (10), 557-565. DOI: 10.1252/jcej.21we009.
- (29) Hirano, T.; Tomonaga, D.; Ogi, T.; Shimokuri, D. Direct spray combustion in a tubular flame burner toward fine particle synthesis. *Journal of Thermal Science and Technology* **2021**, *16* (3), JTST0035-JTST0035. DOI: 10.1299/jtst.2021jtst0035.
- (30) Hirano, T.; Kaseda, S.; Cao, K. L. A.; Iskandar, F.; Tanabe, E.; Ogi, T. Multiple ZnO Core Nanoparticles Embedded in TiO<sub>2</sub> Nanoparticles as Agents for Acid Resistance and UV Protection. *ACS Applied Nano Materials* **2022**, *5* (10), 15449-15456. DOI: 10.1021/acsanm.2c03489.
- (31) Ho, T. T. N.; Hirano, T.; Narui, R.; Tsutsumi, H.; Kishi, M.; Yoshikawa, Y.; Cao, K. L. A.; Ogi, T. Flame-Made Ir–IrO<sub>2</sub>/TiO<sub>2</sub> Particles as Anode Catalyst Support for Improved Durability in Polymer Electrolyte Fuel Cells. *ACS Applied Energy Materials* **2023**, *6* (11), 6064–6071. DOI: 10.1021/acsaem.3c00536.

- (32) Cao, K. L. A.; Kito, Y.; Le, P. H.; Ogi, T.; Hirano, T. Synthesis of Spherical  $\beta$ -Quartz Solid-Solution Particles Derived from Cordierite Using a Flame Process. *ACS Applied Engineering Materials* **2023**, *1* (7), 1789–1798.
- (33) Senoo, Y.; Kakinuma, K.; Uchida, M.; Uchida, H.; Deki, S.; Watanabe, M. Improvements in electrical and electrochemical properties of Nb-doped  $\text{SnO}_{2-\delta}$  supports for fuel cell cathodes due to aggregation and Pt loading. *RSC Adv.* **2014**, *4* (61), 32180-32188. DOI: 10.1039/c4ra03988b.
- (34) Saha, M. S.; Paul, D. K.; Peppley, B. A.; Karan, K. Fabrication of catalyst-coated membrane by modified decal transfer technique. *Electrochem. Commun.* **2010**, *12* (3), 410-413. DOI: 10.1016/j.elecom.2010.01.006.
- (35) Schneider, C. A.; Rasband, W. S.; Eliceiri, K. W. NIH Image to ImageJ: 25 years of image analysis. *Nature methods* **2012**, *9* (7), 671-675.

Supporting Information for

# Porosity Engineering of Pt Loaded Nb–SnO<sub>2</sub> Catalyst Layers in Polymer Electrolyte Fuel Cells

*Tomoyuki Hirano,\*<sup>1</sup> Takama Tsuboi,<sup>1</sup> Thi Thanh Nguyen Ho,<sup>1</sup> Eishi Tanabe,<sup>2</sup> Aoi Takano,<sup>3</sup>  
Mikihiro Kataoka,<sup>3</sup> and Takashi Ogi\*<sup>1</sup>*

<sup>1</sup> Chemical Engineering Program, Graduate School of Advanced Science and Engineering,  
Hiroshima University, 1-4-1 Kagamiyama, Higashi-Hiroshima, Hiroshima 739-8527, Japan

<sup>2</sup> Hiroshima Prefectural Institute of Industrial Science and Technology, 3-10-31 Kagamiyama,  
Higashi Hiroshima, Hiroshima 739-0046, Japan.

<sup>3</sup> Cataler Corporation, 7800 Chihama, Kakegawa, Shizuoka 437-1492, Japan

\*Corresponding Author:

Tomoyuki Hirano; Email: tomoyuki-hirano@hiroshima-u.ac.jp; Phone: +81-82-424-7850

Takashi Ogi; Email: ogit@hiroshima-u.ac.jp; Phone: +81-82-424-3765

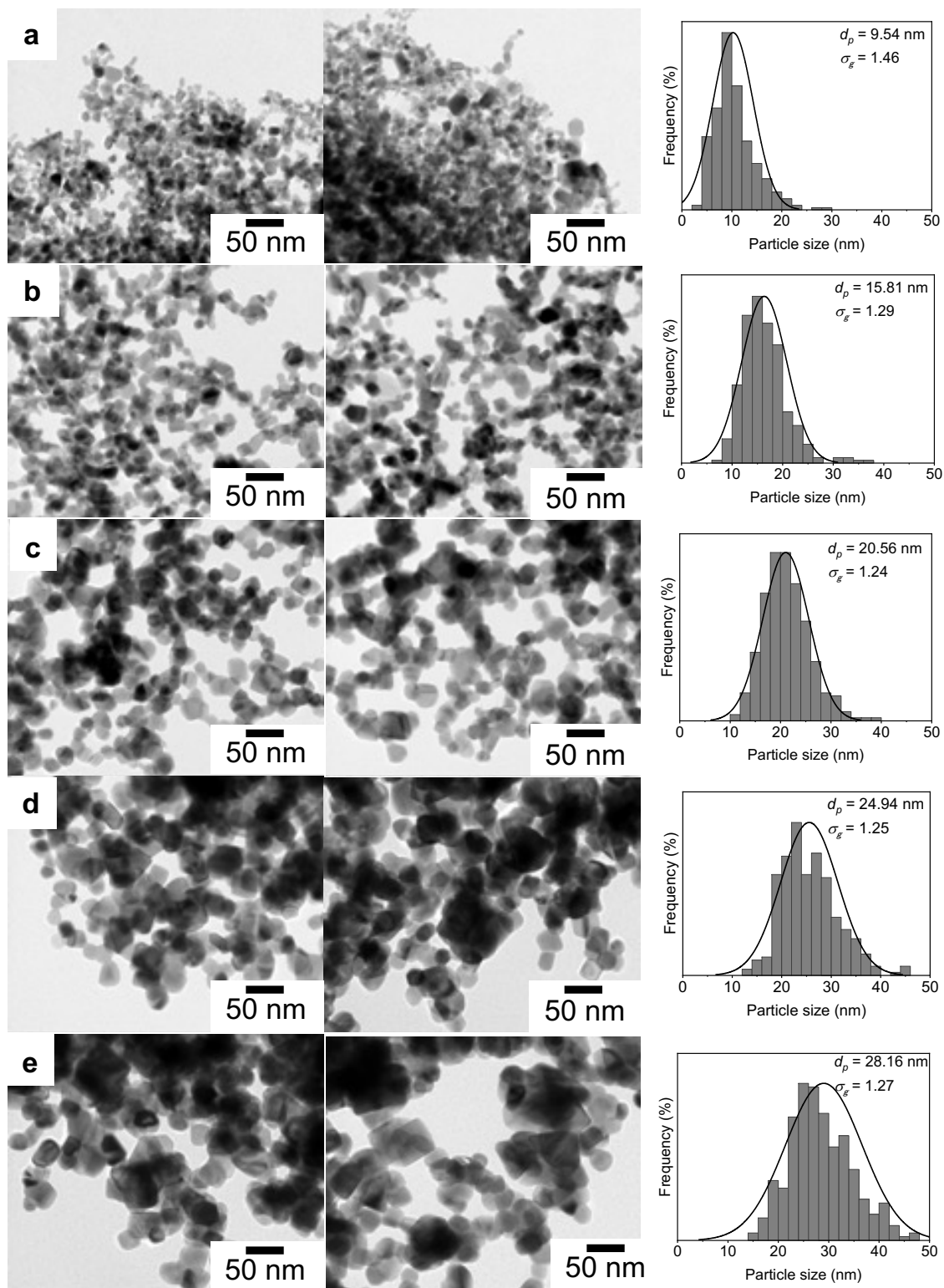


**Figure S1.** TEM images of flame-made NTO nanoparticles (a) before annealing and after annealing at (b) 1000°C for 1 h, (c) at 1200°C for 1 h, (d) at 1200°C for 2 h, and (e) at 1200°C for 4 h. Particle size measurements were performed on >500 particles.